Application of multiconfiguration pair-density functional theory to the Diels-Alder reaction

Erica C. Mitchell,[a,b] Thais R. Scott,[a] Jie J. Bao,[a] and Donald G. Truhlar[a,*]

[a] Department of Chemistry, Chemical Theory Center, and Minnesota Supercomputing Institute, University of Minnesota – Twin Cities, Minneapolis, MN 55455-0931

[b] Department of Chemistry, University of Georgia, Athens, GA 30602

Corresponding author email: truhlar@umn.edu

ABSTRACT. Transition states for Diels-Alder reactions are strongly correlated, as evidenced by high-to-very-high M diagnostics, and therefore they require treatment by multireference methods. Multiconfiguration pair-density functional theory (MC-PDFT) combines a multiconfiguration wave function with a functional of the electron density and the on-top pair density to calculate the electronic energy for strongly correlated systems at a much lower cost than wave function methods that do not employ density functionals. Here we apply MC-PDFT to the Diels-Alder cycloaddition reaction of 1,3-butadiene with ethylene, where two kinds of reaction paths have been widely studied: concerted synchronous paths and diradical stepwise paths. The lowest-energy reaction path is now known to be a concerted synchronous one, and a method's ability to predict this is an important test. By comparison to the best available theoretical results in the literature, we test the accuracy of MC-PDFT with several choices of on-top functional for geometries and enthalpies of stable structures along both paths and for the transition state geometries. We also calculate the Arrhenius activation energies for both paths and compare these to experiment. We also compare to Kohn-Sham density functional theory (KS-DFT) with delected exchange-correlation functionals. CAS-PDFT gives consistently good results for both the concerted and stepwise mechanisms, but none of the KS-DFT functionals gives accurate activation energies for both. The stepwise transition state is very strongly correlated, and MC-PDFT can treat it, but KS-DFT (which involves a single-configuration treatment) has larger errors in the activation energy. This confirms that using a multiconfigurational reference function for strongly correlated transition states can significantly improve the accuracy, and that MC-PDFT can provide this accuracy at a much lower computational cost than competing multireference methods.

Introduction

The Diels-Alder reaction of butadiene and ethylene was at the center of a long-flourishing debate in the chemical community.[1–6] Experimental results were unable to distinguish whether the reaction takes place via a synchronous mechanism in which bonds rearrange simultaneously or by a two-step mechanism where one bond forms first, producing a diradical intermediate structure, and then the second bond forms.[1–3,5,7–11] The controversy over the mechanism was heavily impacted by the increasing capability of quantum mechanical calculations; especially controversial was the contrast between the predictions of semiempirical and *ab initio* methods. Dewar et al. reported a step-wise diradical path which was supported by results from methods such as MINDO/2, MINDO/3, and the modified intermediate neglect of differential overlap.[1,6,12–15] Houk et al. advocated for the concerted synchronous pathway based on restricted Hartree-Fock (RHF) and unrestricted Hartree-Fock (UHF) calculations using STO-3G and 3-21G basis sets.[1,13–16] Each of these kinds of reaction path had computational support from later calculations. Consensus was finally reached in 1986 after Dewar's newer model, Austin Model 1 (AM1),[17] and more complete ab initio studies[1,3,16] converged in predicting a concerted synchronous transition state.

Experimental rate constants from Rowley and Steiner, yielded an Arrhenius activation energy of 27.5 ± 0.5 kcal mol^{-1} at 800 K.[18] The diradical transition state was later estimated to be 2-7 kcal mol^{-1} [2,3,8–10,19] higher than that of the concerted synchronous pathway based on thermochemical analysis and studies of the decomposition of vinylcyclobutane.[5,20] In 2003, Guner et al. compared barrier heights determined from various experimental and theoretical studies. [21] Their compilation included many different theoretical methods, including Hartree-Fock (HF), Møller-Plesset second-order perturbation theory (MP2), complete active space self-consistent field theory (CASSCF), complete active space second-order perturbation theory (CASPT2), the CBS-Q3 composite method of Petersson,[22,23] and a variety of Kohn- Sham density functionals (B3LYP, BPW91, MPW1K, and KMLYP), [21] and it also included a variety of basis sets. Shortly after this, an in-depth analysis with multireference averaged quadratic coupled cluster (MR-AQCC) theory was presented by Lischka et al., and their work is considered to be the most accurate study available and therefore suitable for testing other mehods.[11]

Multiconfiguration pair-density functional theory (MC-PDFT) was introduced in 2014.[24] The method is similar in form to Kohn-Sham density functional theory (KS-DFT) but differs by using a multiconfigurational wave function as the reference and replacing the exchange-correlation functional by an on-top pair-density functional.[24–29] Many studies using MC-PDFT have been done, mainly focused on potential energy curves,[30–32] excited states,[26,33-39] and singlet-triplet splittings.[26,40,41] There has also been research on the application of MC-PDFT to barrier heights[28,40,42,43,44] but only one study[44] included pericyclic reactions. We have recently added MC-PDFT analytic gradients to *OpenMolcas*.[45,46] With these available, the present article investigates the performance of MC-PDFT for describing pericyclic reactions including MC-PDFT geometry optimization of critical structures. In particular, we study the Diels-Alder cycloaddition of ethylene to 1,3-butadiene. MC-PDFT geometry optimizations are done on all structures and compared to the best-estimate MR-AQCC calculations of Lischka et al.[7,11]

Previous studies have shown that the concerted transition state is aromatic[2,9,11,14] and can be well described by using Kohn-Sham density functional theory (KS-DFT), but KS-DFT has not been widely used to study the diradical path. Here, both MC-PDFT and KS-DFT are used on all the Diels–Alder transition states reported by Lischka *et al.* to show the difference between MC-PDFT calculations based on a multiconfiguration wave function and an on-top functional from KS-DFT calculations based on a

Slater determinant and an exchange-correlation functional. Our calculations test whether density functional theory and pair-density functional theory correctly predict the concerted synchronous mechanism to be the lowest-energy path.

Computational methods

All MC-PDFT calculations in this article are CAS-PDFT, i.e., they use a CASSCF calculation as the MCSCF reference function. Starting structures for geometry optimizations were taken from the work of Lischka et al., where they were calculated with MR-AQCC and CASSCF with various Pople basis sets.11 For all structures, starting orbitals for CAS-PDFT came from an initial restricted Hartree-Fock (RHF) calculation.

The geometries were then optimized with CAS-PDFT. The products and transition states employed an active space of 6 active electrons in 6 active orbitals, denoted (6,6), including the π and π^* orbitals and the σ orbitals of the bonds forming during the reaction. Butadiene and ethylene (the reactants) were treated with (4,4) and (2,2) active spaces, respectively, including only π and π^* orbitals. We employed C_1 symmetry for all structures except butadiene which was computed with full C_{2h} symmetry for better convergence of the geometry. Many of the diradical transition states were optimized in two steps, starting with a constrained optimization with the bond formed between ethylene and butadiene frozen to provide a good starting geometry for the second unconstrained step.

The on-top pair-density functional chosen for all MC-PDFT calculations was tPBE. We used six basis sets obtained from the Basis Set Exchange:[47–49] 6-31G**,[50–52] 6-311G(2d,p),[53] 6-31+G**,[50–52,54] cc-pVDZ,[55] jun-cc-pVDZ,[55,56] and jul-cc-pVDZ.[55,56] All CAS-PDFT computations were done using *OpenMolcas,* version 18.09.[57]

The *M* diagnostic[58] was used to characterize the electronic structures at the optimized geometries. An *M* diagnostic uses the natural orbital occupation numbers to compute the degree of multireference character. Three ranges of multireference character are distinguished:[34,58] small ($M < 0.05$), modest ($0.05 \leq M \leq 0.10$), and large ($M > 0.10$). We prefer the M diagnostic over other multireference diagnostics because it is size consistent and because it is a direct measure of the multiconfigurational character of the wave function.

Zero-point energies and thermal rovibrational energies were computed using KS-DFT with *Gaussian 16*[59] because analytic Hessians are not yet available for MC-PDFT. The MN15 exchange-correlation functional[60] with the ma-TZVP[61,62] basis set was chosen for this purpose because it gave the smallest root-mean square deviation from the CAS-PDFT optimized structures. A vibrational scaling[63,64] factor of 0.975[65] was used to improve the accuracy of the zero-point energies.

Conventional transition state theory[66–68] was used to calculate the rate constants as a function of temperature. The rate constants at 790, 800, and 810 K were used to calculate the slope of an Arrhenius plot at 800 K, and this was used to give an Arrhenius activation energy for comparison to experiment. To obtain the free energy of activation, CAS-PDFT electronic energies and MN15/ma-TZVP thermal rovibrational free energies were computed. All thermochemical energy corrections (zero-point energies, thermal rovibrational energies, and thermal rovibrational free energies) used a scale factor of 0.975 for vibrational frequencies and are presented in the Supplementary Information (SI).

KS-DFT calculations with exchange-correlation functionals were also used for this system to compare the enthalpies of reaction and Arrhenius activation energies, both at 800 K. The KS-DFT geometry optimizations had starting structures from Lischka et al. The functionals used included one

local functional, PBE (restricted and unrestricted),[69,70] and several hybrid functionals, MN15,[60] B3LYP,[71,72] M06,[71] revM06,[72] and PBE0.[75,76] For most of the hybrid functionals, we used the aug-cc-pVTZ[55,77] and ma-TZVP[78] basis sets. The PBE, unrestricted PBE (UPBE), and PBE0 calculations were done only with aug-cc-pVTZ except for PBE which also used 6-31G**. PBE/6-31G** was included to provide a comparison to the on-top pair-density functional, tPBE, used for CAS-PDFT. All density functional calculations were done using either *Gaussian 16* or *Gaussian 09* with the *Minnesota Gaussian Functional Module*.[59,78]

Geometries

Figure 1 depicts various conformations in which a σ bond can be formed from the stepwise addition of ethylene to butadiene. The dihedral angle of C_6 (ethylene) with respect to C_2 (butadiene) along the C_5–C_1 bond (ethylene–butadiene), highlighted in Figure 1, is utilized to identify the isomers of the diradical transition states. The diradical geometries are thereby distinguished as anti, eclipsed-in, eclipsed-out, and gauche-out. Transition states are abbreviated TS with the dihedral angle identifier in parentheses, e.g., TS(anti), and intermediates are abbreviated INT with the dihedral identifier in parentheses, e.g., INT(eclipsed-in).

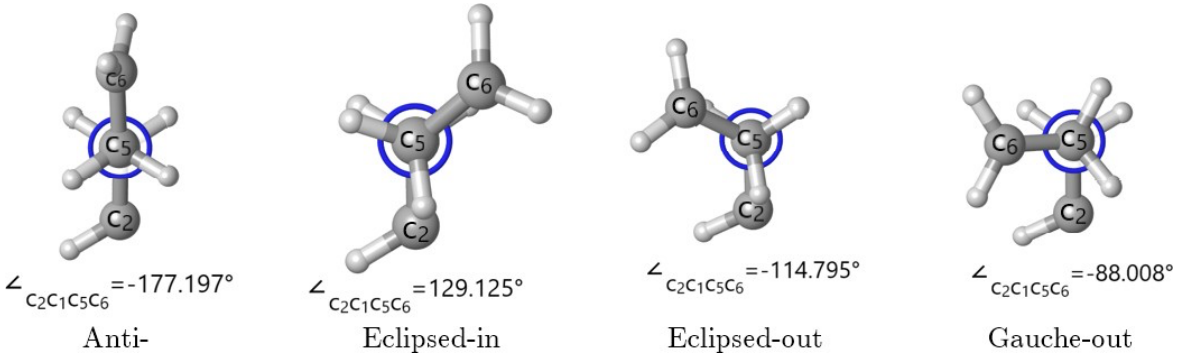

Figure 1: Newman projection of the dihedral angle on the C_1-C_5 bond of the diradical transition states with the atoms and bonds off the dihedral not shown. C_1 and C_2 are a bond of the butadiene while C_5 and C_6 are atoms in the ethylene molecule.

CAS-PDFT/cc-pVDZ optimized geometries are presented in Figure 2. Utilizing CAS-PDFT/cc-pVDZ, one concerted transition state (CTS), four diradical transition states [TS(anti), TS(gauche-out), TS(eclipsed-in), and TS(eclipsed-out)], and two intermediates [INT(anti) and INT(gauche-out)] were located, where the natures of the stationary points are confirmed by the number of imaginary frequencies. With other basis sets, we were unable to converge at least one of the TS structures, in particular TS(gauche-out) [6-31G**, 6-311G(2d,p), 6-31+G**, and jun-cc-pVDZ] and the concerted transition state [6-31+G**, jun-cc-pVDZ, and jul-cc-pVDZ]. The concerted transition state could only be identified using non-diffuse basis sets. In comparison to CAS-PDFT, the KS-DFT calculations were only able to identify the concerted transition state and two diradical transition states [TS(anti) and TS(eclipsed-out)]. Cartesian coordinates for all optimized structures are presented in the SI.

In their study, Lischka *et al.* determined that at the MR-AQCC level, the gauche-in intermediate and transition state did not exist; instead, they found a barrierless pathway to the product and the CTS, respectively. From the geometry optimizations, the only method that agrees with the investigation done by Lischka *et al.*[11] is CAS-PDFT/cc-pVDZ.

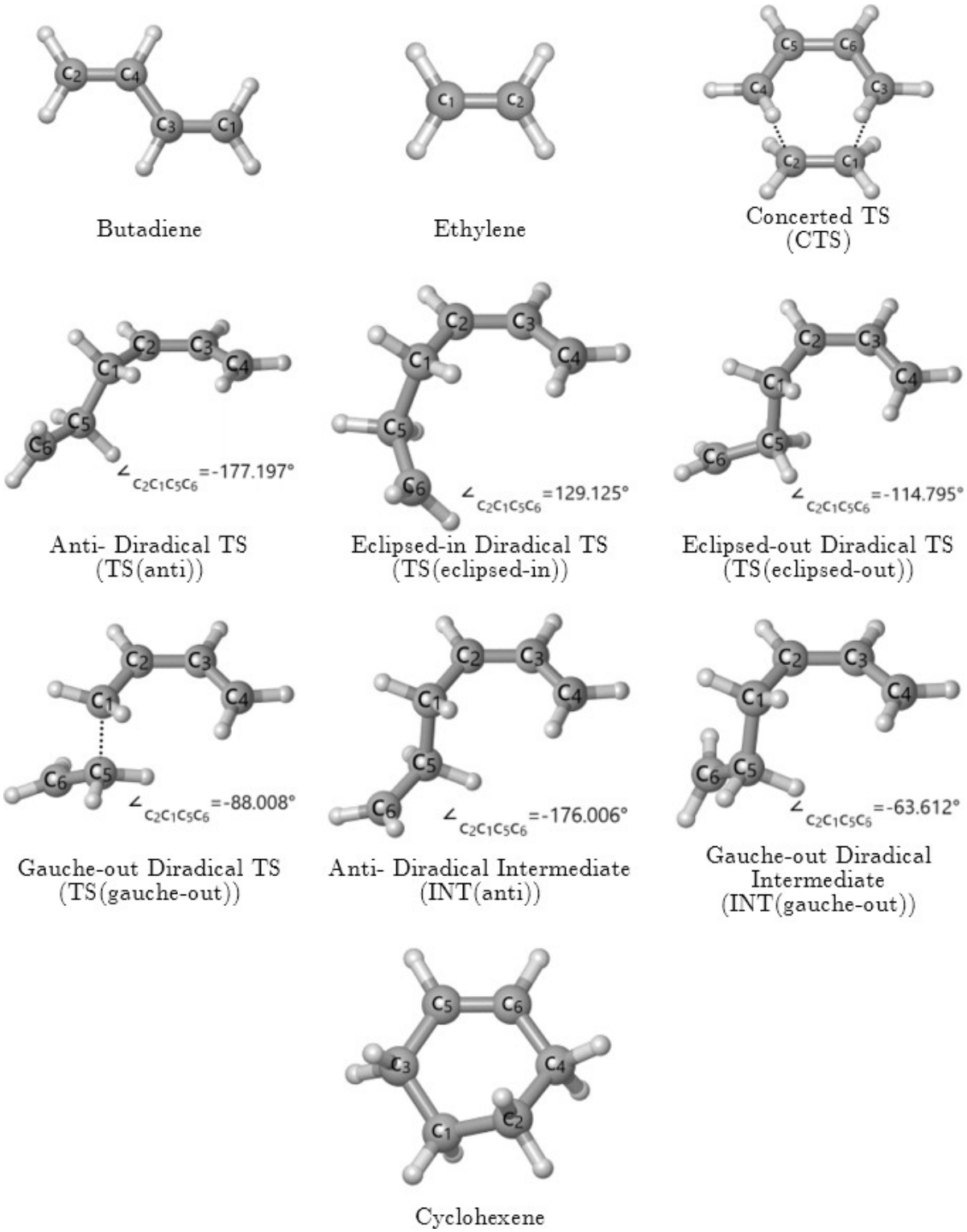

Figure 2: CAS-PDFT/cc-pVDZ geometries with the dihedral angle of $C_2C_1C_5C_6$ shown for the diradical transition states.

Table 1 presents the *M* values for the CASSCF calculations that serve as reference functions for CAS-PDFT/cc-pVDZ (those for other basis sets are presented in the SI). The *M* values of all diradical transition states and intermediates exhibit very large multireference character ($M > 0.5$),

and butadiene and the CTS also exhibit large multireference character ($M > 0.1$). Ethylene and cyclohexene would both be categorized as having modest multireference character ($0.05 \leq M \leq 0.1$). The high M values associated with each geometry further reinforce the need for a multireference method, such as CAS-PDFT, to accurately describe the Diels-Alder reaction.

Table 1: M diagnostics of reactants, transition states, and product of the Diels-Alder reaction calculated by CASSCF/cc-pVDZ.

Molecule	M	HOMO occupation	LUMO occupation
1,3-butadiene	0.118	1.884	0.120
ethylene	0.088	1.912	0.088
CTS	0.135	1.865	0.136
TS(anti)	0.994	1.006	0.994
TS(eclipsed-in)	0.775	1.225	0.776
TS(eclipsed-out)	0.808	1.193	0.808
TS(gauche-out)	0.584	1.416	0.585
INT(anti)	0.803	1.197	0.803
INT(gauche-out)	0.862	1.138	0.862
cyclohexene	0.082	1.918	0.082

Lischka et al. used MR-AQCC to optimize the geometries of the Diels-Alder reaction. We found that CAS-PDFT was able to locate many of the same structures as MR-AQCC. To compare the two methods, the mean unsigned deviation (MUD) of each CAS-PDFT optimized internal coordinate relative to the associated MR-AQCC internal coordinate was calculated, and these MUDs are given in Tables 2 and 3. In each case we compared to the MR-AQCC results for the largest basis set for which the particular structure was optimized; in particular that means we compared to MR-AQCC/6-311G(2d,1p) structures for reactants, product, and CTS, to MR-AQCC/6-31G** structures for TS(anti), INT(anti), TS(eclipsed-in), and TS(eclipsed-out), and to MR-AQCC/6-31G* structures for TS(gauche-out) and INT(gauche-out).

Table 2: MUD of the dihedral angles for the CAS-PDFT transition states compared to the MR-AQCC geometries from Lischka et al.[a]

Basis set for CAS-PDFT	MUD of CTS (degrees)	MUD of TS(anti) (degrees)
6-31G**	1.00	1.00
6-311G(2d,p)	0.99	1.69
cc-pVDZ	1.00	20.01

[a] The CTS dihedral angles included in this error calculation are: C_4-C_2-C_1-C_3, C_6-C_3-C_1-C_2, C_5-C_4-C_2-C_1, H_1-C_6-C_3-C_1, H_2-C_5-C_4-C_2, H_3-C_3-C_1-C_2, H_4-C_4-C_2-C_1, H_5-C_3-C_1-C_2, H_6-C_4-C_2-C_1, H_7-C_1-C_2-C_3, H_8-C_2-C_1-C_3, H_9-C_1-C_2-C_3, and H_{10}-C_2-C_1-C_3. The TS(anti) dihedral angles included in this error

calculation are: C_4-C_3-C_2-C_1, C_5-C_1-C_2-C_3, C_6-C_5-C_1-C_2, H_1-C_1-C_2-C_3, H_2-C_1-C_2-C_3, H_3-C_2-C_1-C_3, H_4-C_3-C_2-C_1, H_5-C_4-C_3-C_2, H_6-C_4-C_3-C_2, H_7-C_5-C_1-C_2, H_8-C_5-C_1-C_2, H_9-C_6-C_5-C_1, and H_{10}-C_6-C_5-C_1.

Table 3: MUD of the dihedral angles for the KS-DFT transition states compared to the MR-AQCC geometries from Lischka et al. [a]

Basis Set	MUD of CTS (degree)	MUD of TS(anti) (degree)
PBE/6-31G**	1.22	13.6
PBE/aug-cc-pVTZ	1.16	14.2
PBE0/aug-cc-pVTZ	0.86	14.0
MN15/ma-TZVP	0.37	15.0
MN15/aug-cc-pVTZ	0.46	15.0
B3LYP/ma-TZVP	0.81	15.4
B3LYP/aug-cc-pVTZ	0.84	15.4
M06/ma-TZVP	0.44	15.6
M06/aug-cc-pVTZ	0.47	15.5
M06-2X/ma-TZVP	0.44	15.0
M06-2X/aug-cc-pVTZ	0.45	15.1
revM06/ma-TZVP	0.33	14.7
revM06/aug-cc-pVTZ	1.22	14.7

[a] The CTS dihedral angles included in this error calculation are: C_4-C_2-C_1-C_3, C_6-C_3-C_1-C_2, C_5-C_4-C_2-C_1, H_1-C_6-C_3-C_1, H_2-C_5-C_4-C_2, H_3-C_3-C_1-C_2, H_4-C_4-C_2-C_1, H_5-C_3-C_1-C_2, H_6-C_4-C_2-C_1, H_7-C_1-C_2-C_3, H_8-C_2-C_1-C_3, H_9-C_1-C_2-C_3, and H_{10}-C_2-C_1-C_3. The TS(anti) dihedral angles included in this error calculation are: C_4-C_3-C_2-C_1, C_5-C_1-C_2-C_3, C_6-C_5-C_1-C_2, H_1-C_1-C_2-C_3, H_2-C_1-C_2-C_3, H_3-C_2-C_1-C_3, H_4-C_3-C_2-C_1, H_5-C_4-C_3-C_2, H_6-C_4-C_3-C_2, H_7-C_5-C_1-C_2, H_8-C_5-C_1-C_2, H_9-C_6-C_5-C_1, and H_{10}-C_6-C_5-C_1.

The most important reaction paths for the Diels-Alder reaction were determined to pass through the CTS and TS(anti) transition states. We show the MUDs of the internuclear distances of these two pathways in Figures 3, 4, and 5.

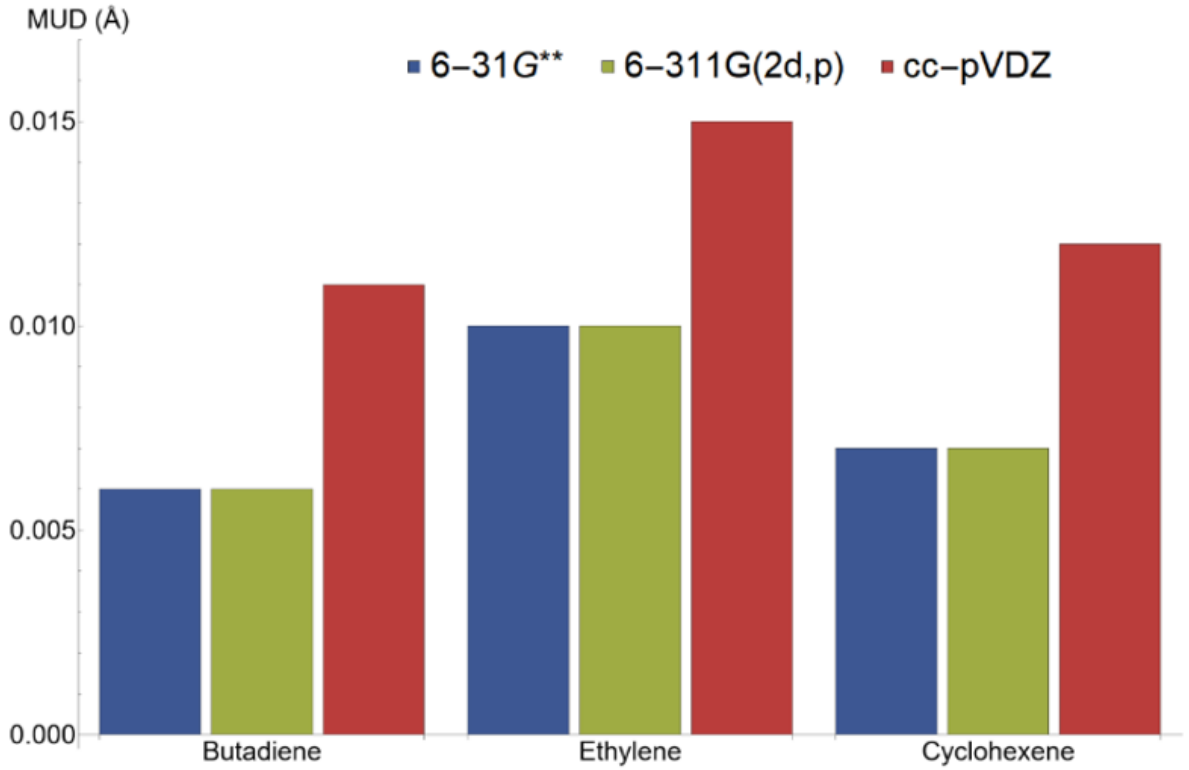

Figure 3: MUD of the internuclear distances (Å) for the CAS-PDFT geometries compared to the MR-AQCC geometries from Lischka et al. The butadiene internuclear distances included in this error calculation are: C_2-C_1, C_3-C_1, C_4-C_2, H_1-C_1, H_2-C_2, H_3-C_1, H_4-C_2, H_5-C_4, and H_6-C_3. The ethylene internuclear distances included in this error calculation are: C_2-C_1, H_1-C_1, H_2-C_2, H_3-C_2, and H_4-C_1. The cyclohexene internuclear distances included in this error calculation are: C_2-C_1, C_3-C_1, C_4-C_2, C_5-C_3, C_6-C_5, H_1-C_5, H_2-C_6, H_3-C_3, H_4-C_4, H_5-C_3, H_6-C_4, H_7-C_1, H_8-C_2, H_9-C_1, and H_{10}-C_2.

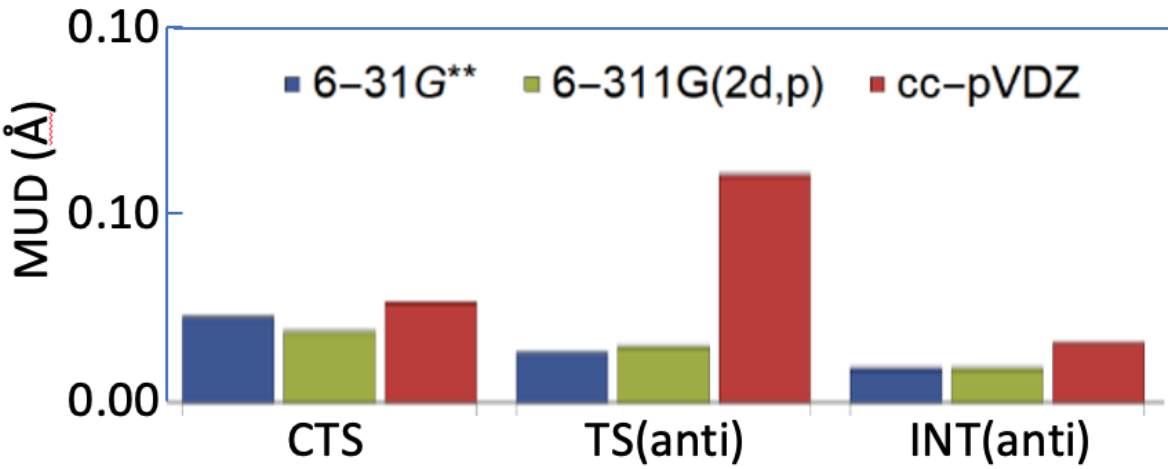

Figure 4: MUD of the internuclear distances (Å) for the CAS-PDFT geometries compared to the MR-AQCC geometries from Lischka et al. The CTS internuclear distances included in this error

calculation are: C_2-C_1, C_3-C_1, C_4-C_2, C_6-C_3, C_5-C_4, H_1-C_6, H_2-C_5, H_3-C_3, H_4-C_4, H_5-C_3, H_6-C_4, H_7-C_1, H_8-C_2, H_9-C_1, and H_{10}-C_2. The TS(anti) and INT(anti) internuclear distances included in this error calculation are: C_2-C_1, C_3-C_2, C_4-C_3, C_5-C_1, C_6-C_5, H_1-C_1, H_2-C_1, H_3-C_2, H_4-C_3, H_5-C_4, H_6-C_4, H_7-C_5, H_8-C_5, H_9-C_6, and H_{10}-C_6.

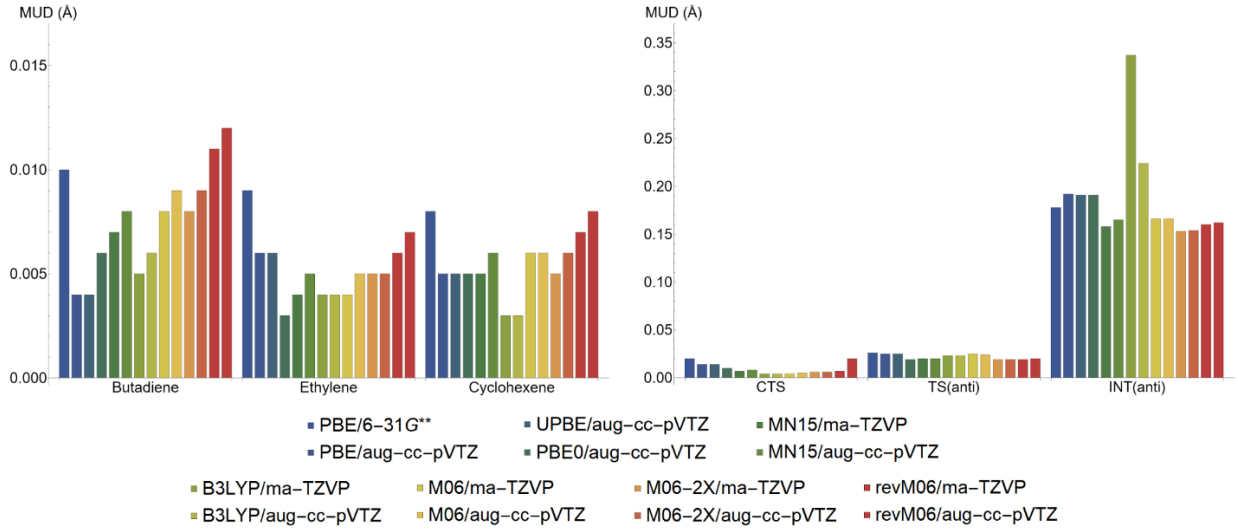

Figure 5: MUD of the internuclear distances (Å) for the KS-DFT geometries compared to the MR-AQCC geometries from Lischka *et al.* The butadiene internuclear distances included in this error calculation are: C_2-C_1, C_3-C_1, C_4-C_2, H_1-C_1, H_2-C_2, H_3-C_1, H_4-C_2, H_5-C_4, and H_6-C_3. The ethylene internuclear distances included in this error calculation are: C_2-C_1, H_1-C_1, H_2-C_2, H_3-C_2, and H_4-C_1. The CTS internuclear distances include: C_2-C_1, C_3-C_1, C_4-C_2, C_6-C_3, C_5-C_4, H_1-C_6, H_2-C_5, H_3-C_3, H_4-C_4, H_5-C_3, H_6-C_4, H_7-C_1, H_8-C_2, H_9-C_1, and H_{10}-C_2. The TS(anti) and INT(anti) internuclear distances included in this error calculation are: C_2-C_1, C_3-C_2, C_4-C_3, C_5-C_1, C_6-C_5, H_1-C_1, H_2-C_1, H_3-C_2, H_4-C_3, H_5-C_4, H_6-C_4, H_7-C_5, H_8-C_5, H_9-C_6, and H_{10}-C_6. The cyclohexene internuclear distances included in this error calculation are: C_2-C_1, C_3-C_1, C_4-C_2, C_5-C_3, C_6-C_5, H_1-C_5, H_2-C_6, H_3-C_3, H_4-C_4, H_5-C_3, H_6-C_4, H_7-C_1, H_8-C_2, H_9-C_1, and H_{10}-C_2.

In the SI, we show the MUD of the internuclear distances, bond angles, and dihedral angles for all geometries. In addition, basis sets in which the CAS-PDFT structures were not located are omitted in Figures 3 and 4 but included in the SI.

Table 2 shows that for CTS, all three basis sets have an MUD for the dihedral-angles of 1.0 deg. The TS(anti) structures have similar dihedral-angle MUDs except for the cc-pVDZ outlier. The largest difference of the CAS-PDFT/cc-pVDZ geometry from the others is that the dihedral angle of the hydrogens on the C_6 atom is more parallel to the C_1-C_5 axis.

In Figures 3 and 4, the MUDs of the internuclear distances for all species are under 0.05 Å. The reactants and product have the lowest MUD ($<$ 0.015 Å). These species show little variance in their MUD with changes in the basis set on the scale of hundredths of an Angstrom. The transition states have slightly increased MUD values, but they still fall under 0.05 Å. This shows that CAS-PDFT performs similarly to MR-AQCC for critical geometries of these reactions.

Table 3 displays the MUDs of the dihedral angles of our KS-DFT optimized structures with respect to the MR-AQCC geometries. All functionals have an MUD of the dihedrals that is $\leq$ 1.23 deg for the

CTS. We note that functionals using the fully augmented aug-cc-pVTZ basis set have a slightly higher MUD than those using the minimally augmented ma-TZVP basis set for CTS. For the TS(anti) structure, the MUD of the dihedral angles is much higher, with the average being 14.8 deg. The higher MUD for TS(anti) is attributed to the diradical nature of the transition state being poorly described by the single-reference KS-DFT functionals.

The MUDs of the KS-DFT bond distances are shown in Figure 5; they are all under 0.027 Å for the reactants, transition states, and product. The MUD of INT(anti) is, on average, 0.19 Å with the largest value being 0.34 Å and the smallest being 0.15 Å. The increased value for the MUD of the internuclear distances for the INT(anti) is due to bond between C_1 and C_5 (the σ bond forming). Lischka et al.'s MR-AQCC/6-31G** INT(anti) C_1-C_5 bond distance (1.60 Å) is much shorter than the computed bond distance for all the KS-DFT geometries, which is 3.91 Å on average.

Arrhenius Energies of Activation and Reaction Enthalpies at 800 K

There are numerous studies on the concerted synchronous path of the Diels-Alder reaction, but Rowley and Steiner's measured Arrhenius activation energy (27.5±0.5 kcal mol^{-1} at 800 K)[18] is generally taken as the most accurate. Figure 6 shows this value as a horizontal line and compares it to the calculated activation energies (calculated as described in the computational methods section) at 800 K from the CAS-PDFT and KS-DFT calculations for reaction through the CTS.

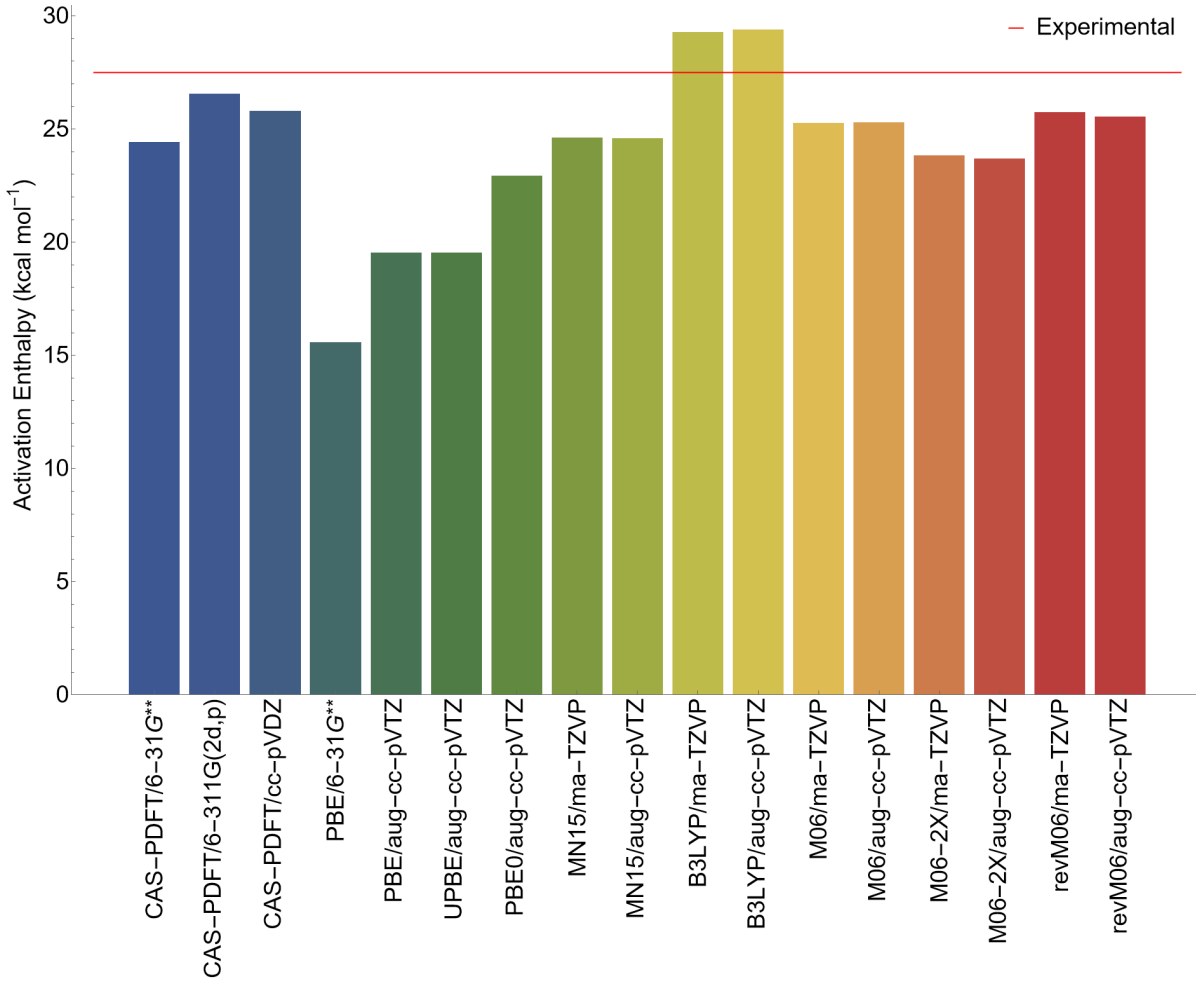

Figure 6: Calculated activation enthalpies of the CTS at various levels of theory.

The CAS-PDFT activation energies with all three basis sets shown agree with experiment within 3 kcal/mol, with CAS-PDFT/6-311G(2d,p) being the most accurate (26.6 kcal mol^{-1}) and within chemical accuracy. In contrast the KS-DFT results differ from experiment by up to 12 kcal/mol. It is encouraging that the multireference CAS-PDFT calculations agree with experiment better than many of the single-reference KS-DFT ones. The performance of MC-PDFT with tPBE is much better than the performance of KS-DFT with PBE or PBE0, although the performance of KS-DFT with better functionals, such as revM06, is comparable to MC-PDFT with PBE.

Much less research has focused on the stepwise path, and because of that, the energy of activation at 800 K is only estimated to be in a range of 2-7 kcal mol^{-1} [2,3,8–10,19] above the Arrhenius activation energy measured by Rowley and Steiner for the concerted path, i.e., to be in the range 29.5-34.5 kcal mol^{-1}. Figure 7 shows this range as a shaded area and compares it to calculated Arrhenius activation energies at 800 K (again calculated as described in the computational methods section). We consider any computed activation energy within the shaded area to be consistent with experiment. In contrast to the CTS activation energies, the hybrid functionals significantly overestimate the energy of activation – on average by 10 kcal mol^{-1}. This failure of KS-DFT is consistent with the much larger *M* diagnostics for the TS(anti) state than for the CTS one in Table 1. A key finding is that CAS-PDFT is the only method of those examined that gives consistently good results for both mechanisms.

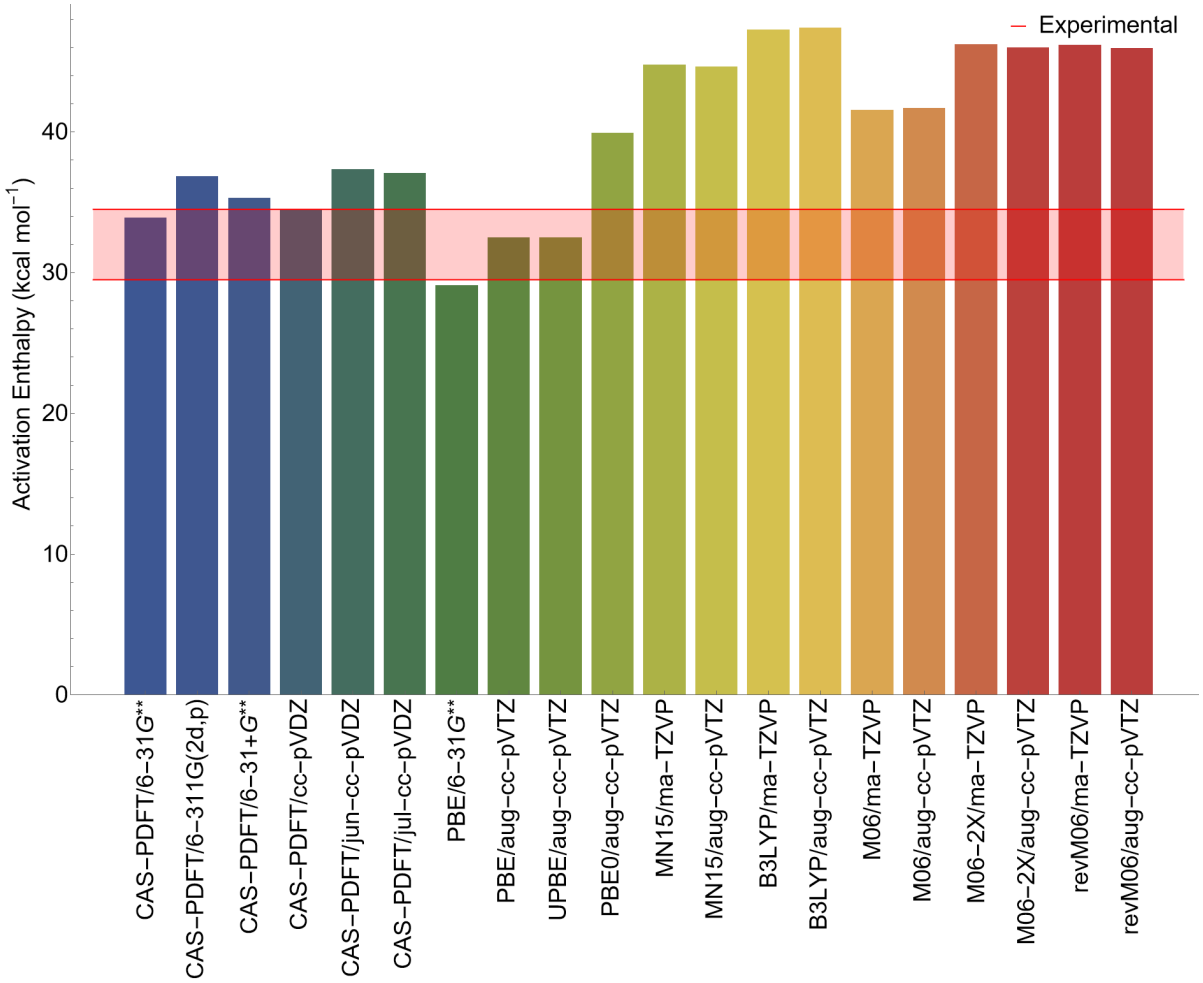

Figure 7: Calculated activation enthalpies of the TS(anti) at various levels of theory. Experimental value is estimated to be 2-7 kcal mol^{-1} above the CTS.[13]

Figure 8 shows our calculations of the reaction enthalpy at 800 K. The experimental reaction enthalpy comes from neutral gas-phase thermodynamic data from the National Institute of Standards and Technology (NIST).[79] The heats of formation from NIST for butadiene, ethylene, and cyclohexene at 298.15 K are 26.00, 12.52, and –1.03 kcal mol^{-1}, respectively, and when adjusted for temperature, the enthalpy of reaction is −40.55 kcal mol^{-1} at 800 K. CAS-PDFT with the various basis sets disagrees with experiment by about 1 to 8 kcal mol^{-1}, with an average error of 3.2 kcal mol^{-1}. KS-DFT differs from the experiment values by about 0.1 to 10.3 kcal mol^{-1}, with an average error of only 3.0 kcal mol^{-1}. We see that, on average, KS-DFT provides slightly more accurate reaction enthalpies for this system. The most accurate Kohn-Sham functionals are MN15 and revM06.

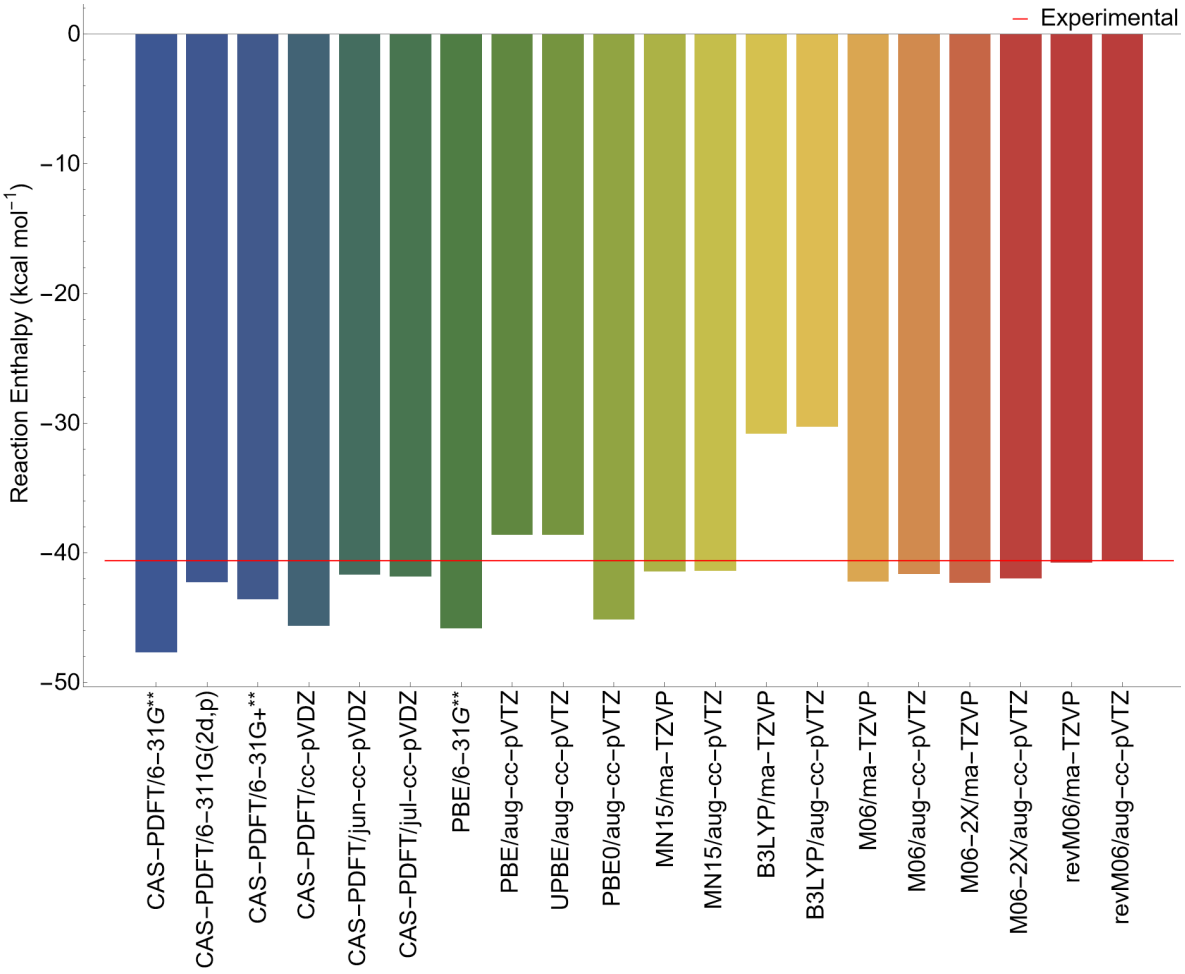

Figure 8: Calculated reaction enthalpies at 800 K at various levels of theory.

Additional Comparisons

As an additional set of comparisons, we calculated single-point energies by CAS-PDFT/jun-cc-pVTZ and NEVPT2/6-311G(2d,p) at the at the geometries used for CAS-PDFT/6-311G(2d,p) in Figures 6 and 7. The results are in Table 4.

As compared to the 6-311G(2d,p) basis set, the jun-c-pVTZ basis set includes diffuse s, p, and d basis functions on the carbon atoms, tight f functions on carbons, and tight d functions on hydrogens.[81] Table 4 shows that the use of this extended basis set raises the calculated enthalpies of activation, but

the 10 kcal/mol difference in the CTS and TS(anti) activation enthalpies falls with the range of 10–12 kcal/mol range obtained with three listed non-diffuse basis sets.

The NEVPT2[82] (n-electron valence states for multireference perturbation theory) calculations show the effect of using the much more expensive multireference perturbation theory instead of MC-PDFT. We used the 6-311G(2d,p) basis set because that basis set was used for the optimized geometries. When using the same basis set, MC-PDFT agrees with experiment better than NEVPT2 for the CTS transition state, but the opposite occurs for the TS(anti) transition state.

Table 4: Enthalpies of activation at 800 K.

	MC-PDFT/				NEVPT2/	Exp.
	6-31G**	6-311G(2d,p)	cc-pVDZ	jun-cc-pVTZ[a]	6-311G(2d,p)[a]	
CTS[b]	24.2	26.6	25.8	29.4	23.9	27.5
TS(anti)[c]	33.9	36.9	37.4	39.7	36.4	29.5–34.5

[a] The jun-cc-pVTZ and NEVPT2 calculations use the geometry from MC-PDFT/6-311G(2d,p). The zero-point energy and thermal contributions to the enthalpy are calculated with MN15/ma-TZVP with a vibrational frequency scale factor of 0.975.

[b] the concerted transition state

[c] the stepwise transition state in the *anti* conformation

Conclusions

This study shows that CAS-PDFT predicts reliable geometries for both stable structures and transition state structures for the Diels-Alder reaction of butadiene and ethylene. We find that CAS- PDFT and KS-DFT provide similar structures as compared to MR-AQCC, but CAS-PDFT is more accurate at computing the structure of INT(anti) and possibly TS(anti).

The Arrhenius energies of activation at 800 K were computed for the two main reaction paths. Although CAS-PDFT and KS-DFT provide similar geometries, only CAS-PDFT can provides an accurate energy of activation for both possible reaction paths. The poor results for KS-PDFT can be traced to the large multireference character of the stepwise transition state. We therefore recommend MC-PDFT for calculating energies of strongly correlated transition states.

The calculated enthalpies of reaction at 800 K show wide variations with basis set and functional, but they are slightly more accurate on average by KS-DFT than by MC-PDFT.

AUTHOR INFORMATION

Corresponding Author

Donald G. Truhlar − Department of Chemistry, Chemical Theory Center, and Minnesota Supercomputing Institute, University of Minnesota, Minneapolis, Minnesota 55455-0431, United States; orcid.org/0000-0002-7742-7294; Email: truhlar@umn.edu

Authors

Erica C. Mitchell – Department of Chemistry, Chemical Theory Center, and Minnesota Supercomputing Institute, University of Minnesota, Minneapolis, Minnesota 55455-0431, United States and Department of Chemistry, University of Georgia, Athens, GA 30602, United States

Thais R. Scott − Department of Chemistry, Chemical Theory Center, and Minnesota Supercomputing Institute, University of Minnesota, Minneapolis, Minnesota 55455-0431, United States

Jie J. Bao − Department of Chemistry, Chemical Theory Center, and Minnesota Supercomputing Institute, University of Minnesota, Minneapolis, Minnesota 55455-0431, United States; orcid.org/0000-0003-0197-3405

Acknowledgment

The authors are grateful to Laura Gagliardi for co-advising the project and to Andrew Sand for contributions to *OpenMolcas* that made the project possible. We thank the University of Minnesota's Summer Undergraduate Research Fellowship in Computational and Theoretical Chemistry (SURF-CTC) and the Summer Lando/NSF REU (Grant No. CHE-1851990) for funding. We thank the Minnesota Supercomputing Institute for computing resources. T.R.S. acknowledges that this material is based on the work supported by the National Science Foundation Graduate Research Fellowship Program under Grant No. CON-75851, Project No. 00074041. This work was also supported in part by the National Science Foundation under grant CHE-2054723. The opinions, findings, conclusions, and recommendations expressed in this article are those of the authors and do not necessarily reflect the views of the National Science Foundation.

Supporting Information Available

The supporting information contains: Cartesian coordinates of optimized CAS-PDFT geometries, CAS-PDFT electronic energies, MN15/ma-TZVP thermochemical corrections, reaction enthalpies at 800 K, activation enthalpies at 800 K, and MUD values for the diradical transition states.

References

(1) Houk, K. N.; Gonzalez, J.; Li, Y. Pericyclic reaction transition states: Passions and punctilios, 1935-1995. *Acc. Chem. Res.* **1995**, *28*, 81–90.

(2) Wiest, O.; Montiel, D. C.; Houk, K. N. Quantum mechanical methods and the interpretation and prediction of pericyclic reaction mechanisms. *J. Phys. Chem. A* **1997**, *101*, 8378–8388.

(3) Houk, K. N.; Li, Y.; Storer, J.; Raimondi, L.; Beno, B. Concerted and stepwise mechanisms in cycloaddition reactions: potential surfaces and isotope effects. *J. Chem. Soc. Faraday Trans.* **1994**, *90*, 1599–1604.

(4) Gregoritza, M.; Brandl, F. P. The Diels–Alder reaction: a powerful tool for the design of drug delivery systems and biomaterials. *Eur. J. Pharm. Biopharm.* **2015**, *97*, 438–453.

(5) Li, Y.; Houk, K. Diels-Alder dimerization of 1, 3-butadiene: an ab initio CASSCF study of the concerted and stepwise mechanisms and butadiene-ethylene revisited. *J. Am. Chem. Soc.* **1993**, *115*, 7478–7485.

(6) Houk, K. N.; Li, Y.; Evanseck, J. D. Transition structures of hydrocarbon pericyclic reactions. *Angew. Chem. Int. Ed.* **1992**, *31*, 682–708.

(7) Scarborough, D. L.; Kobayashi, R.; Thompson, C. D.; Izgorodina, E. I. Active space and basis set effects in CASPT2 models of the 1,3-butadiene-ethene cycloaddition and the 1, 3-butadiene dimerization. *Int. J. Quantum Chem.* **2015**, *115*, 989–1001.

(8) Goldstein, E.; Beno, B.; Houk, K. Density functional theory prediction of the relative energies and isotope effects for the concerted and stepwise mechanisms of the Diels- Alder reaction of butadiene and ethylene. *J. Am. Chem. Soc.* **1996**, *118*, 6036–6043.

(9) Sakai, S. Theoretical analysis of concerted and stepwise mechanisms of Diels-Alder reaction between butadiene and ethylene. *J. Phys. Chem. A* **2000**, *104*, 922–927.

(10) Isobe, H.; Takano, Y.; Kitagawa, Y.; Kawakami, T.; Yamanaka, S.; Yamaguchi, K.; Houk, K. Systematic Comparisons between Broken Symmetry and Symmetry-Adapted Approaches to Transition States by Chemical Indices: A Case Study of the Diels- Alder Reactions. *J. Phys. Chem. A* **2003**, *107*, 682–694.

(11) Lischka, H.; Ventura, E.; Dallos, M. The Diels–Alder Reaction of Ethene and 1,3-Butadiene: An Extended Multireference ab initio Investigation. *ChemPhysChem* **2004**, *5*, 1365–1371.

(12) Dewar, M. J.; Griffin, A. C.; Kirschner, S. MINDO/3 study of some Diels-Alder reactions. *J. Am. Chem. Soc.* **1974**, *96*, 6225–6226.

(13) Townshend, R.; Ramunni, G.; Segal, G.; Hehre, W.; Salem, L. Organic transition states. V. The Diels-Alder reaction. *J. Am. Chem. Soc.* **1976**, *98*, 2190–2198.

(14) Bernardi, F.; Bottoni, A.; Field, M. J.; Guest, M. F.; Hillier, I. H.; Robb, M. A.; Venturini, A. MC-SCF study of the Diels-Alder reaction between ethylene and butadiene. *J. Am. Chem. Soc.* **1988**, *110*, 3050–3055.

(15) Brown, F. K.; Houk, K. The STO-3G transition structure of the Diels-Alder reaction. *Tetrahedron Lett.* **1984**, *25*, 4609–4612.

(16) Dewar, M. J.; Olivella, S.; Stewart, J. J. Mechanism of the Diels-Alder reaction: reactions of butadiene with ethylene and cyanoethylenes. *J. Am. Chem. Soc.* **1986**, *108*, 5771–5779.

(17) Dewar, M. J.; Zoebisch, E. G.; Healy, E. F.; Stewart, J. J. Development and use of quantum mechanical molecular models. 76. AM1: A new general purpose quantum mechanical molecular model. *J. Am. Chem. Soc.* **1985**, *107*, 3902–3909.

(18) Rowley, D.; Steiner, H. Kinetics of diene reactions at high temperatures. *Discuss. Faraday Soc.* **1951**, *10*, 198–213.

(19) Isobe, H.; Takano, Y.; Kitagawa, Y.; Kawakami, T.; Yamanaka, S.; Yamaguchi, K.; Houk, K. Extended Hartree-Fock (EHF) theory of chemical reactions VI: hybrid DFT and post-Hartree-Fock approaches for concerted and non-concerted transition structures of the Diels-Alder reaction. *Mol. Phys.* **2002**, *100*, 717–727.

(20) Frey, H. M.; Pottinger, R. Thermal unimolecular reactions of vinylcyclobutane and isopropenylcyclobutane. *J. Chem. Soc. Faraday Trans. I* **1978**, *74*, 1827–1833.

(21) Guner, V.; Khuong, K. S.; Leach, A. G.; Lee, P. S.; Bartberger, M. D.; Houk, K. A standard set of pericyclic reactions of hydrocarbons for the benchmarking of computational methods: the performance of ab initio, density functional, CASSCF, CASPT2, and CBS-QB3 methods for the prediction of activation barriers, reaction energetics, and transition state geometries. *J. Phys. Chem. A* **2003**, *107*, 11445–11459.

(22) Montgomery Jr, J. A.; Frisch, M. J.; Ochterski, J. W.; Petersson, G. A. A complete basis set model chemistry. VI. Use of density functional geometries and frequencies. *J. Chem. Phys.* **1999**, *110*, 2822–2827.

(23) Montgomery Jr, J. A.; Frisch, M. J.; Ochterski, J. W.; Petersson, G. A. A complete basis set model chemistry. VII. Use of the minimum population localization method. *J. Chem. Phys.* **2000**, *112*, 6532–6542.

(24) Li Manni, G.; Carlson, R. K.; Luo, S.; Ma, D.; Olsen, J.; Truhlar, D. G.; Gagliardi, L. Multiconfiguration pair-density functional theory. *J. Chem. Theory Comput.* **2014**, *10*, 3669–3680.

(25) Gagliardi, L.; Truhlar, D. G.; Li Manni, G.; Carlson, R. K.; Hoyer, C. E.; Bao, J. L. Multiconfiguration pair-density functional theory: A new way to treat strongly correlated systems. *Acc. Chem. Res.* **2017**, *50*, 66–73.

(26) Sharma, P.; Bernales, V.; Truhlar, D. G.; Gagliardi, L. Valence $\pi\pi^*$ excitations in benzene studied by multiconfiguration pair-density functional theory. *J. Phys. Chem. Letters* **2018**, *10*, 75–81.

(27) Ghosh, S.; Verma, P.; Cramer, C. J.; Gagliardi, L.; Truhlar, D. G. Combining wave function methods with density functional theory for excited states. *Chem. Rev.* **2018**, *118*, 7249–7292.

(28) Sand, A. M.; Kidder, K. M.; Truhlar, D. G.; Gagliardi, L. Calculation of Chemical Reaction Barrier Heights by Multiconfiguration Pair-Density Functional Theory with Correlated Participating Orbitals. *J. Phys. Chem. A* **2019**, *123*, 9809–9817.

(29) Sand, A. M.; Truhlar, D. G.; Gagliardi, L. Efficient algorithm for multiconfiguration pair-density functional theory with application to the heterolytic dissociation energy of ferrocene. *J. Chem. Phys.* **2017**, *146*, 034101.

(30) Zhou, C.; Gagliardi, L.; Truhlar, D. G. State-interaction pair density functional theory for locally avoided crossings of potential energy surfaces in methylamine. *Phys. Chem. Chem. Phys.* **2019**, *21*, 13486–13493.

(31) Li, S. J.; Gagliardi, L.; Truhlar, D. G. Extended separated-pair approximation for transition metal potential energy curves. *J. Chem. Phys.* **2020**, *152*, 124118.

(32) Oakley, M. S.; Bao, J. J.; Klobukowski, M.; Truhlar, D. G.; Gagliardi, L. Multireference methods for calculating the dissociation enthalpy of tetrahedral P_4 to two P_2. *J. Phys. Chem. A* **2018**, *122*, 5742–5749.

(33) Ghosh, S.; Sonnenberger, A. L.; Hoyer, C. E.; Truhlar, D. G.; Gagliardi, L. Multiconfiguration pair-density functional theory outperforms Kohn–Sham density functional theory and multireference perturbation theory for ground-state and excited-state charge transfer. *J. Chem. Theory Comput.***2015**, *11*, 3643–3649.

(34) Bao, J. J.; Gagliardi, L.; Truhlar, D. G. Multiconfiguration pair-density functional theory for doublet excitation energies and excited state geometries: the excited states of CN. *Phys. Chem. Chem. Phys.* **2017**, *19*, 30089–30096.

(35) Bao, J. J.; Dong, S. S.; Gagliardi, L.; Truhlar, D. G. Automatic selection of an active space for calculating electronic excitation spectra by MS-CASPT2 or MC-PDFT. *J. Chem. Theory Comput.***2018**, *14*, 2017–2025.

(36) Hoyer, C. E.; Ghosh, S.; Truhlar, D. G.; Gagliardi, L. Multiconfiguration pair-density functional theory is as accurate as CASPT2 for electronic excitation. *J. Phys. Chem. Lett.* **2016**, *7*, 586–591.

(37) Bao, J. J.; Truhlar, D. G. Automatic Active Space Selection for Calculating Electronic Excitation Energies Based on High-Spin Unrestricted Hartree-Fock Orbitals. *J. Chem. Theory Comput.* **2019**, *15*, 5308–5318.

(38) Ning, J.; Truhlar, D. G. The valence and Rydberg states of dienes. *Phys. Chem. Chem. Phys.* **2020**, *22*, 6176–6183.

(39) Dong, S. S.; Gagliardi, L.; Truhlar, D. G. Nature of the 1^1Bu and 2^1Ag excited states of butadiene and the Goldilocks principle of basis set diffuseness. *J. Chem. Theory Comput.* **2019**, *15*, 4591–4601.

(40) Ghosh, S.; Cramer, C. J.; Truhlar, D. G.; Gagliardi, L. Generalized-active-space pair-density functional theory: an efficient method to study large, strongly correlated, conjugated systems. *Chem. Sci.* **2017**, *8*, 2741–2750.

(41) Stoneburner, S. J.; Truhlar, D. G.; Gagliardi, L. MC-PDFT can calculate singlet-triplet splittings of organic diradicals. *J. Chem. Phys.* **2018**, *148*, 064108.

(42) Carlson, R. K.; Li Manni, G.; Sonnenberger, A. L.; Truhlar, D. G.; Gagliardi, L. Multiconfiguration pair-density functional theory: Barrier heights and main group and transition metal energetics. *J. Chem. Theory Comput.* **2015**, *11*, 82– 90.

(43) Carlson, R. K.; Truhlar, D. G.; Gagliardi, L. Multiconfiguration pair-density functional theory: a fully translated gradient approximation and its performance for transition metal dimers and the spectroscopy of $Re2Cl_8^{2-}$. *J. Chem. Theory Comput.* **2015**, *11*, 4077–4085.

(44) Odoh, S. O.; Manni, G. L.; Carlson, R. K.; Truhlar, D. G.; Gagliardi, L. Separated-pair approximation and separated-pair pair-density functional theory. *Chem. Sci.* **2016**, *7*, 2399–2413.

(45) Sand, A. M.; Hoyer, C. E.; Sharkas, K.; Kidder, K. M.; Lindh, R.; Truhlar, D. G.; Gagliardi, L. Analytic gradients for complete active space pair-density functional theory. *J. Chem. Theory Comput.* **2018**, *14*, 126–138.

(46) Scott, T. R.; Hermes, M. R.; Sand, A. M.; Oakley, M. S.; Truhlar, D. G.; Gagliardi, L. Analytic gradients for state-averaged multiconfiguration pair-density functional theory. *J. Chem. Phys.* **2020**, *153*, 014106.

(47) Feller, D. The role of databases in support of computational chemistry calculations. *J. Comp. Chem.* **1996**, *17*, 1571–1586.

(48) Schuchardt, K. L.; Didier, B. T.; Elsethagen, T.; Sun, L.; Gurumoorthi, V.; Chase, J.; Li, J.; Windus, T. L. Basis set exchange: A community database for computational sciences. *J. Chem. Inf. Model.* **2007**, *47*, 1045–1052.

(49) Pritchard, B. P.; Altarawy, D.; Didier, B.; Gibson, T. D.; Windus, T. L. New basis set exchange: An open, up-to-date resource for the molecular sciences community. *J. Chem. Inf. Model.* **2019**, *59*, 4814–4820.

(50) Ditchfield, R.; Hehre, W. J.; Pople, J. A. Self-consistent molecular-orbital methods. IX. An extended Gaussian-type basis for molecular-orbital studies of organic molecules. *J. Chem. Phys.* **1971**, *54*, 724–728.

(51) Hariharan, P. C.; Pople, J. A. The influence of polarization functions on molecular orbital hydrogenation energies. *Theor. Chim. Acta* **1973**, *28*, 213–222.

(52) Hehre, W. J.; Ditchfield, R.; Pople, J. A. Self-consistent molecular orbital methods. XII. Further extensions of Gaussian-type basis sets for use in molecular orbital studies of organic molecules. *J. Chem. Phys.* **1972**, *56*, 2257–2261.

(53) Krishnan, R.; Binkley, J. S.; Seeger, R.; Pople, J. A. Self-consistent molecular orbital methods. XX. A basis set for correlated wave functions. *J. Chem. Phys.* **1980**, *72*, 650–654.

(54) Clark, T.; Chandrasekhar, J.; Spitznagel, G. W.; Schleyer, P. V. R. Efficient diffuse function-augmented basis sets for anion calculations. III. The 3-21+G basis set for first-row elements, Li–F. *J. Comp. Chem.* **1983**, *4*, 294–301.

(55) Dunning Jr, T. H. Gaussian basis sets for use in correlated molecular calculations. I. The atoms boron through neon and hydrogen. *J. Chem. Phys.* **1989**, *90*, 1007–1023.

(56) Papajak, E.; Leverentz, H. R.; Zheng, J.; Truhlar, D. G. Efficient Diffuse Basis Sets: cc-pVxZ+ and maug-cc-pVxZ. *J. Chem. Theory Comput.* **2009**, *5*, 1197–1202.

(57) Fdez. Galván, I.; Vacher, M.; Alavi, A.; Angeli, C.; Aquilante, F.; Autschbach, J.; Bao, J. J.; Bokarev, S. I.; Bogdanov, N. A.; Carlson, R. K.; et al. OpenMolcas: From Source Code to Insight. *J. Chem. Theory Comput.* **2019**, *15*, 5925–5964.

(58) Tishchenko, O.; Zheng, J.; Truhlar, D. G. Multireference model chemistries for thermochemical kinetics. *J. Chem. Theory Comput*. **2008**, 4, 1208–1219.

(59) Frisch, M. J.; Trucks, G. W.; Schlegel, H. B.; Scuseria, G. E.; Robb, M. A.; Cheeseman, J. R.; Scalmani, G.; Barone, V.; Petersson, G. A.; Nakatsuji, H.; et al. Gaussian 16, Revision C.01, Gaussian, Inc., Wallingford CT, 2016.

(60) Yu, H. S.; He, X.; Li, S. L.; Truhlar, D. G. MN15: A Kohn-Sham global-hybrid exchange–correlation density functional with broad accuracy for multi-reference and single-reference systems and noncovalent interactions. *Chem. Sci.* **2016**, *7*, 5032–5051.

(61) Zheng, J.; Xu, X.; Truhlar, D. G. Minimally augmented Karlsruhe basis sets. *Theor. Chem. Acc.* **2011**, *128*, 295–305.

(62) Weigend, F.; Ahlrichs, R. Balanced basis sets of split valence, triple zeta valence and quadruple zeta valence quality for H to Rn: Design and assessment of accuracy. *Phys. Chem. Chem. Phys.* **2005**, *7*, 3297–3305.

(63) Alecu, I.; Zheng, J.; Zhao, Y.; Truhlar, D. G. Computational thermochemistry: scale factor databases and scale factors for vibrational frequencies obtained from electronic model chemistries. *J. Chem. Theory Comput.* **2010**, *6*, 2872–2887.

(64) Haoyu, S. Y.; Fiedler, L. J.; Alecu, I.; Truhlar, D. G. Computational thermochemistry: Automated generation of scale factors for vibrational frequencies calculated by electronic structure model chemistries. *Computer Phys. Commun.* **2017**, *210*, 132–138.

(65) Kanchanakungwankul, S.; Bao, J.; Zheng, J.; Alecu, I.; Lynch, B.; Zhao, Y.; Truhlar, D. G. Database of Frequency Scale Factors for Electronic Model Chemistries-Version 4. https://comp.chem.umn.edu/freqscale/ (accessed July 17, 2019)

(66) Truhlar, D. G.; Hase, W. L.; Hynes, J. T. Current status of transition-state theory. *J. Phys. Chem.* **1983**, *87*, 2664–2682.

(67) Kreevoy, M.; Truhlar, D. G. Transition State Theory. In *Investigation of Rates and Mechanisms of Reactions*; 4th edition, edited by C. F. Bernasconi; John Wiley and Sons: New York, 1986; Part 1, pp. 13-95.

(68) Truhlar, D. G.; Garrett, B. C. Variational transition-state theory. *Acc. Chem. Res.* **1980**, *13*, 440–448.

(69) Perdew, J. P.; Burke, K.; Ernzerhof, M. Generalized gradient approximation made simple. *Phys. Rev. Lett.* **1996**, *77*, 3865–3868.

(70) Perdew, J. P.; Burke, K.; Ernzerhof, M. Errata: Generalized Gradient Approximation Made Simple. *Phys. Rev. Lett.* **1997**, *78*, 1396.

(71) Becke. A. Becke's three parameter hybrid method using the LYP correlation functional. *J. Chem. Phys.* **1993**, *98*, 5648–5652.

(72) Stephens, P. J.; Devlin, F. J.; Chabalowski, C. F.; Frisch, M. J. *Ab Initio* Calculation of Vibrational Absorption and Circular Dichroism Spectra Using Density Functional Force Fields. *J. Phys. Chem.* **1994**, *98*, 11623-11627.

(73) Zhao, Y.; Truhlar, D. G. The M06 suite of density functionals for main group thermochemistry, thermochemical kinetics, noncovalent interactions, excited states, and transition elements: two new functionals and systematic testing of four M06-class functionals and 12 other functionals. *Theor. Chem. Acc.* **2008**, *120*, 215–241.

(74) Wang, Y.; Verma, P.; Jin, X.; Truhlar, D. G.; He, X. Revised M06 density functional for main-group and transition-metal chemistry. *Proc. Nat. Acad. Sci.* **2018**, *115*, 10257–10262.

(75) Adamo, C.; Barone, V. Toward reliable density functional methods without adjustable parameters: The PBE0 model. *J. Chem. Phys.* **1999**, *110*, 6158–6170.

(76) Ernzerhof, M.; Scuseria, G. E. Assessment of the Perdew–Burke–Ernzerhof exchange-correlation functional. *J. Chem. Phys.* **1999**, *110*, 5029–5036.

(77) Kendall, R. A.; Dunning Jr, T. H.; Harrison, R. J. Electron affinities of the first-row atoms revisited. Systematic basis sets and wave functions. *J. Chem. Phys.* **1992**, *96*, 6796–6806.

(78) Zheng, J.; Xu, X.; Truhlar, D. G. Minimally augmented Karlsruhe basis sets. *Theor. Chem. Acc.* **2011***, 128*, 295−305.

(79) Zhao, Y.; Peverati, R.; Yang, R.; Luo, S.; Yu, H.; He, X.; Truhlar, D. Minnesota- Gaussian functional module (MN-GFM, version 6.5), http://comp.chem.umn.edu/mn-gfm (accessed June 16, 2019)

(80) Afeefy, H. Y.; Liebman, J. F.; Stein, S. E. "Neutral Thermochemical Data" in NIST Chemistry WebBook, NIST Standard Reference Database Number 69, Eds. P. J. Linstrom and W. G. Mallard, National Institute of Standards and Technology, Gaithersburg MD, 20899, https://doi.org/10.18434/T4D303 (accessed June 16, 2019).

(81) Papajak, E.; Truhlar, D. G. Convergent Partially Augmented Basis Sets for Post-Hartree-Fock Calculations of Molecular Properties and Reaction Barrier Heights. *J. Chem. Theory Comput.* **2011**, *7*, 10–18.

(82) Angeli, C.; Cimiraglia, R.; Evangelisti, S.; Leininger, T.; Malrieu, J. -P. Introduction of n-electron valence states for multireference perturbation theory. *J. Chem. Phys.* **2001***, 114*, 10252.

TOC graphic